NONLINEAR FINITE ELEMENT ANALYSIS OF COMPOSITE CONCRETE BEAMS

Prof. Dr. Khalid S. Mahmoud Dr. Mohannad H. Al-Sherrawi
Dept. of Civil Engineering,
University of Baghdad , Iraq

ABSTRACT

To study the nonlinear response of composite concrete beams, a finite element analysis is presented. Material nonlinearities as a result of nonlinear response of concrete in compression, crushing and cracking of concrete, strain softening and stiffening after cracking, yielding of reinforcement, bond-slip, shear-slip, and dowel action between the precast concrete beams and the cast-in-situ slabs are considered.

A biaxial concrete model is adopted. Concrete is treated as an orthotropic material with smeared rotating crack model. The steel reinforcement is assumed to be in a uniaxial stress state and is modeled as a bilinear material.

A two-dimensional plane stress finite element type is used to model the concrete. Reinforcement is represented by one-dimensional bar elements. Bond-slip and dowel action is modeled by using fictitious linkage elements with two springs at right angles. Shear-slip is modeled by using shear transfer interface elements with appropriate stiffness values.

Comparison between the results obtained by the finite element and available experimental results of composite concrete beams is made. The results compare satisfactorily with the experimental ones.

الخلاصة

لغرض معرفة مقدار تحمل الأعتاب الخرسانية المركبة و استجابتها اللاخطية للأحمال الستاتيكية المؤثرة عليها ، تم تحليلها بواسطة الحاسبة الإلكترونية و باستعمال طريقة العناصر المحددة. عدة علاقات لاخطية اعتمدت ، كالعلاقة اللاخطية بين الإجهاد و الانفعال لمادة الخرسانة ، كذلك لمادة الحديد ، العلاقة بين قوة الربط و الانزلاق بين حديد التسليح و مادة الخرسانة المحيطة به ، العلاقة بين قوى القص و الانزلاق الحاصل عند سطح التماس بين العتبة المسبقة الصب و خرسانة الأرضية المصبوبة موقعياً ، و كذلك التأثير الوتدي لرابطات القص.

بالنسبة للخرسانة تم اعتماد نموذج العلاقات التكوينية للمادة المختلفة بالاتجاهين المتعامدين. و تم تمثيل التشقق في الخرسانة بطريقة الشقوق الموزعة الدوارة. تم اعتبار حديد التسليح ذو مواصفات أحادية الاتجاه و باتجاه قضبان التسليح.

لتمثيل الخرسانة تم استعمال عنصر الإجهاد المستوي عند تحليل العتبة المركبة بطريقة العناصر المحددة. حديد التسليح مُثل بعنصر أحادي الاتجاه. و لتمثيل الربط والانزلاق و التاثير الوتدي تم استعمال عنصر وصلي ذو نابضين متعامدين. قوى القص و الانزلاق مُثلت بعنصر السطح البيني.

تم عمل مقارنة بين النتائج المستحصلة في هذه الدراسة مع ما هو متوفر من نتـــائج للفحـــوص المختبريـــة لاعتاب خرسانية مركبة. النتائج المستحصلة كانت مقاربة للنتائج المختبرية.

KEYWORDS
composite beams, nonlinear analysis, orthotropic material, finite element, shear-slip.

INTRODUCTION

The composite concrete beam or girder usually consists of a precast or cast-in-situ reinforced or prestressed concrete beam and a cast-in-place reinforced concrete slab tied together to act as a unit. The shear connectors between the beam and the slab should tie the components together well enough so that they act as a monolithic T-beam. Typical section of building and bridge composite reinforced concrete flexural beam is shown in **Fig. (1).**

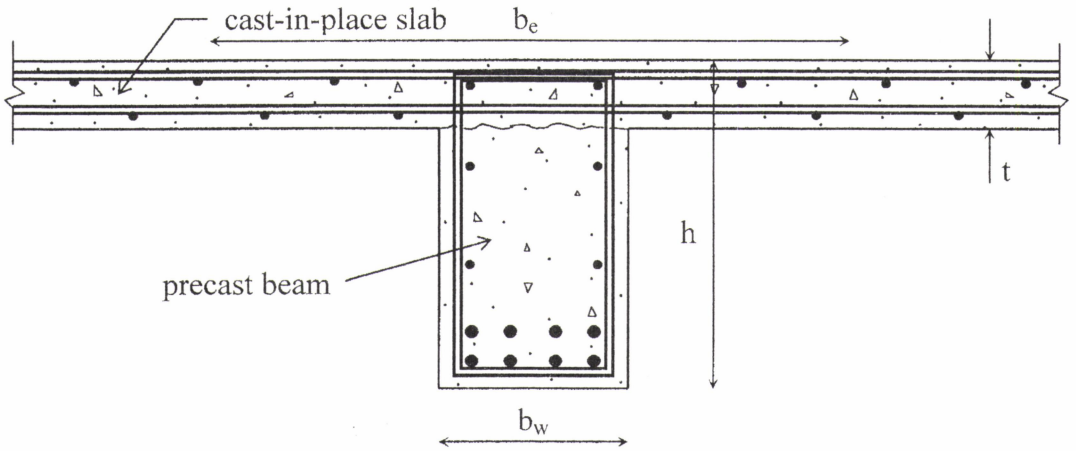

Fig. (1) Typical composite reinforced concrete beam.

MECHANICAL PROPERTIES

To model a reinforced concrete specimen, it is not only necessary to model the concrete and the steel correctly but their interaction as well. This involves the tension stiffening effect in concrete due to bond slip between the concrete and steel and the effect of dowel action and shear due to the reinforcement.

Concrete

To model nonlinear concrete response, the constitutive relation contained in the modified compressive field theory (Vecchio and Collins, 1986), **Fig. (2)** has been adopted. Thus, for concrete in compression, the relation is:

$$\sigma_c = f_c' \left[2\left(\frac{\varepsilon_c}{\varepsilon_o}\right) - \left(\frac{\varepsilon_c}{\varepsilon_o}\right)^2 \right] \qquad (1)$$

where σ_c and ε_c are the average principal compressive stress and strain in concrete, respectively; ε_o is the strain in concrete cylinder at peak stress f_c'.

For concrete in tension, prior to cracking, a linear relation is used:

$$\sigma_t = E_c \cdot \varepsilon_t \qquad 0 \le \varepsilon_t \le \varepsilon_{cr} \qquad (2)$$

where

$$E_c = \frac{2f_c'}{\varepsilon_o} \qquad \varepsilon_{cr} = \frac{f_{cr}}{E_c} \qquad f_{cr} = 0.33\sqrt{f_c'} \quad \text{(in MPa)}$$

and σ_t and ε_t are the average principal tensile stress and strain in concrete, respectively; E_c is the modulus of elasticity of concrete (initial tangent stiffness); f_{cr} and ε_{cr} are concrete cracking stress and strain, respectively.

After cracking, concrete in tension is made to reflect tension softening and tension stiffening effects together through the following relation:

$$\sigma_t = \frac{f_{cr}}{1+\sqrt{200\varepsilon_t}} \qquad (3)$$

ζ_σ :stress softening coefficient of concrete.

ζ_ε :strain softening coefficient of concrete.

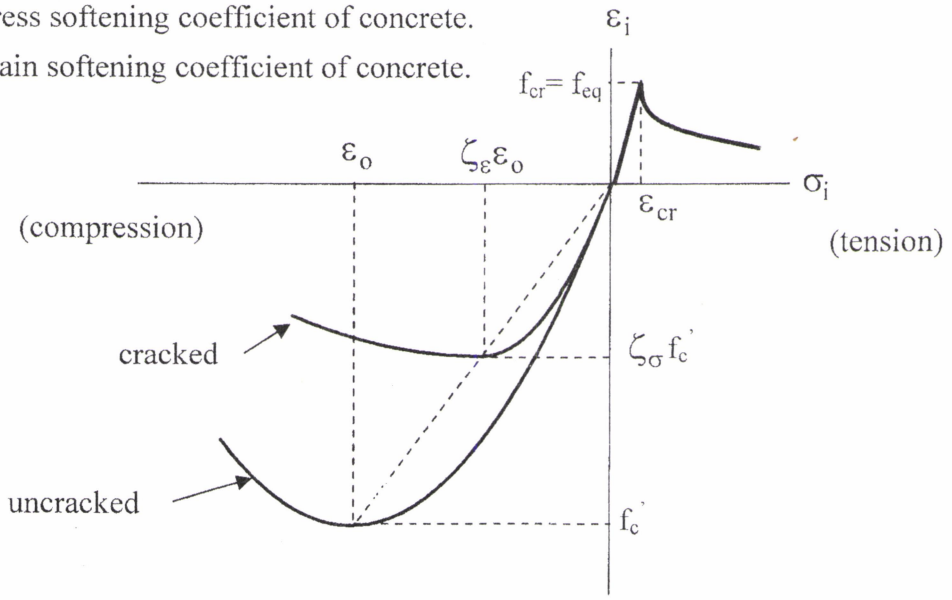

Fig. (2) Stress-strain relation adopted.

Reinforcing Steel

The bilinear representation of the stress-strain relation of the steel reinforcement is found adequate for the proper simulation of the actual behavior since the elastic-plastic behavior with or without the introduction of the strain-hardening region is easily simulated by controlling the slope of the second line.

Friction Slip and Separation

In current design practice, the surface between two concrete parts cast at different ages is a plane of weakness in an otherwise monolithic beam. In addition to tensile strength, this surface is usually characterized by the Coulomb friction parameters, namely cohesion and a coefficient of friction. In the ACI Code "Building Code Requirements for Structural Concrete (ACI 318M-95)", for a crack being assumed along an interface, tensile strength and cohesion are considered to be zero while the coefficient of friction (μ) is assumed dependent on the concrete placement. For example, μ=1.4 for concrete placed monolithically, μ=1.0 for concrete placed against hardened concrete with

surface intentionally roughened, μ=0.6 for concrete placed against hardened concrete not intentionally roughened.

For normal stresses (σ_n) ranging up to 2 MPa, Fronteddu et al. (1998) utilized their experimental results from displacement controlled shear tests on concrete lift joint specimens with different surface preparations, to propose an empirical interface constitutive model based on the concept of basic friction coefficient (μ_b) and roughness friction coefficient (μ_i):

$$\mu = \frac{\lambda_d \mu_b + \chi_i \mu_i}{1 - \lambda_d \chi_i \mu_b \mu_i} \qquad (4)$$

where $\square_b = 0.950\text{-}0.220\ \square_n$ for $\sigma_n \leq 0.5\text{MPa}$

$\square_b = 0.865\text{-}0.050\ \square_n$ for $0.5 \leq \sigma_n \leq 2.0\text{MPa}$

λ_d is the dynamic reduction factor equal to 1.00 for static loading and 0.85 for dynamic loading, and χ_i is the interface roughness factor equal to 1.00 for cracked homogeneous concrete, 0.80 for water-blasted joints, 0.15 for untreated joints, and 0.00 for flat independent concrete surfaces.

Based on the experimental results presented by Fronteddu et al. (1998), a bilinear relationship between shearing stress and slip is adopted, **Fig. (3).**

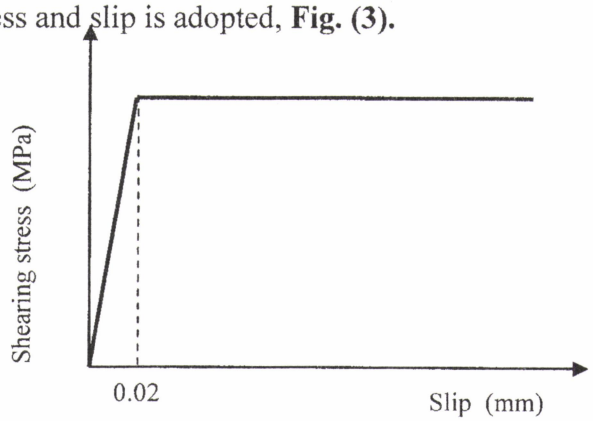

Fig. (3) Adopted shearing stress-slip relationship.

Dowel Action:

Shear force can be transmitted across a crack in reinforced concrete by the reinforcement crossing the crack. If the reinforcement is normal to the plane of cracking, dowel action (shearing and flexure of the bars) will contribute to the over-all shear stiffness. With oblique reinforcement there is also a contribution from the tangential component of the axial force in the reinforcement.

The efficiency of dowel action in shear transfer in cracked reinforced concrete structures depends strongly on the confinement exerted by the surrounding concrete, as well as on the hoop action of the stirrups.

It has been suggested (Paulay et al, 1974) that there are three mechanisms of shear transfer through dowel action in cracked reinforced concrete, i.e. direct shear, kinking and flexure of the bars. If the concrete supporting each bar were considered rigid, the first two mechanisms would predominate. However, it has been recognized (Mills, 1975) that significant deformation of the concrete does occur, so that flexure of the dowel bar within the concrete is a principal action.

The experimental data presented by Poli et al. (1993) will be utilized to propose the following simplified mathematical model for the secant stiffness of dowel action against core (k_d):

$$k_d = \frac{20 + 5(d_b - 14)}{1.5} \qquad |\Delta| \le 1.5 \text{ mm}$$

$$k_d = \frac{20 + 5(d_b - 14)}{|\Delta|} \qquad |\Delta| \ge 1.5 \text{ mm} \qquad (5)$$

where d_b is the diameter of the bar; and Δ is the dowel displacement. These equations are shown in **Fig. (4).**

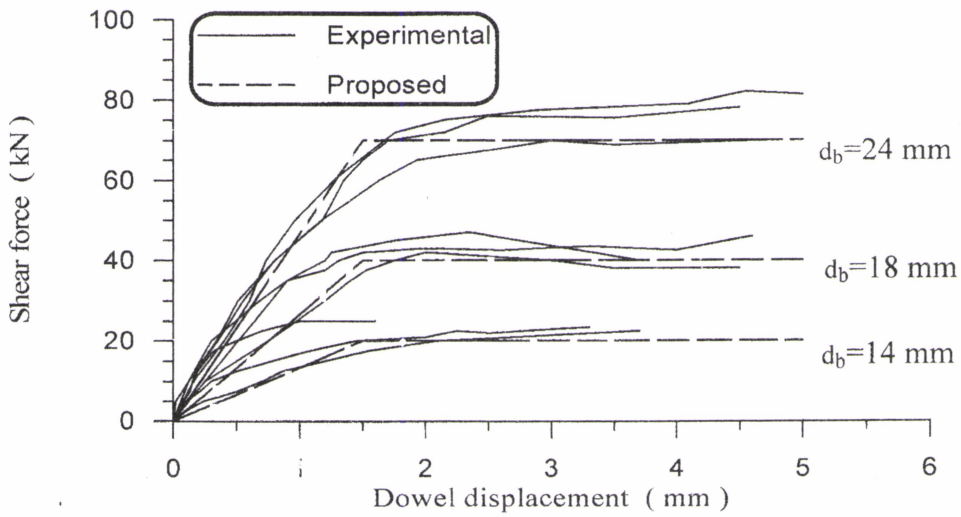

Fig. (4) Proposed dowel stiffness.

Bond Stress-Slip Relation

Based on the experimental results presented by Darwin and Graham (1993), a bilinear relationship between bond stress and bond slip is adopted, **Fig. (5).** The mathematical model for the secant stiffness of bond-slip is:

$$k_s = 25 \qquad |\Delta_s| \le 0.2\text{mm}$$

$$k_s = \frac{5}{|\Delta_s|} \qquad |\Delta_s| \ge 0.2\text{mm} \qquad (6)$$

where k_s is the secant stiffness for bond-slip; and ϕ is the slip.

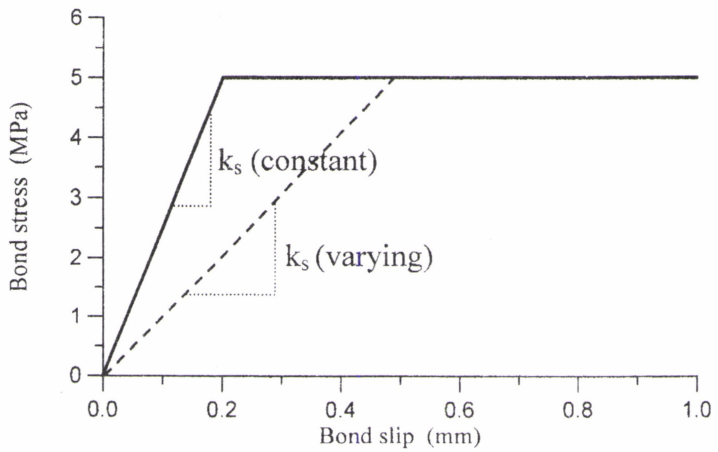

Fig. (5) Adopted bond stress-bond slip relationship.

FINITE ELEMENT REPRESENTATION

For simplicity it is preferable to approximate the original three-dimensional problem to an equivalent two-dimensional one when possible.

A finite element with two-dimensional plane stress element type is used to model the concrete **Fig. (6).** The rotating smeared crack model is used for modeling cracking. Reinforcement is represented by one-dimensional bar elements. Bond-slip and dowel action are modeled by using fictitious linkage elements, **Fig. (7).** Shear-slip is modeled by using shear transfer interface elements with appropriate stiffness values, **Fig. (8).**

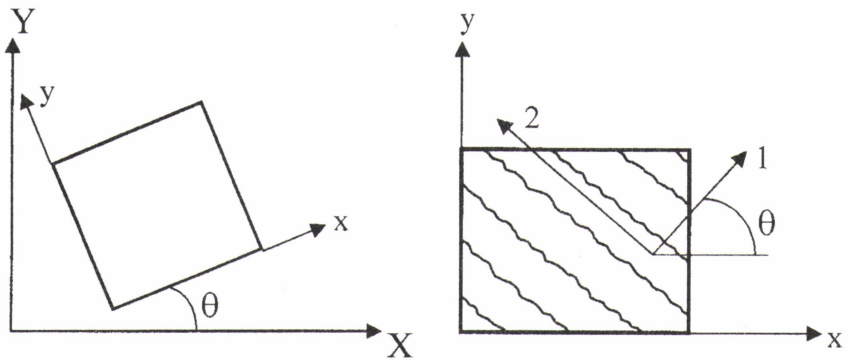

(a) (b)

Fig. (6) Four-noded quadrilateral element (a) element in global coordinates, (b) cracked element.

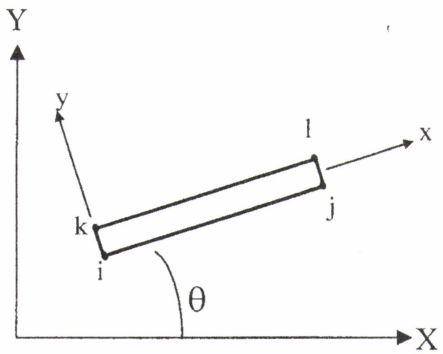

Fig. (7) Interface element.

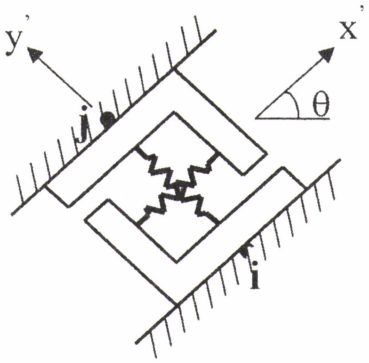

Fig. (8) Linkage element.

To achieve the requirements of the present work, a computer program (MHND) has been written based on the orthotropic concrete constitutive models (Al-Sherrawi, 2000). It is coded in Microsoft Visual Basic 6.0. The equation solver is based on symmetric banded Gaussian Elimination.

The nonlinear material properties considered in the present analysis are:

1- Nonlinear stress-strain relationship of concrete.
2- Cracking of concrete.
3- Yielding of reinforcement.
4- Bond slip.
5- Post-cracking shear transfer by aggregate interlock and dowel action.
6- Friction slip.
7- Separation.

An incremental-iterative technique and the secant stiffness approach were utilized as a solution algorithm. The local stiffness matrices are updated on the second iteration of every increment, rather than the first. This is very helpful since the local stiffness matrices are calculated only after load increment has been applied, i.e. the global stiffness matrix of the structure is evaluated on the basis of the actual stress present at that increment, rather than on the basis of the previously reached stress state.

ANALYSIS OF COMPOSITE CONCRETE BEAMS

Several experimental investigations of composite concrete beams are available in the literature. although some of the available tests have concentrated only on specific aspects of the structural problem and their experimental data are usually incomplete. In this paper, the computer program (MHND) is used to analyze several composite concrete beams, which were tested by others, and comparisons between the experimental and the finite element results are given.

Saemann and Washa tests:

The evaluation of the strength of the joint between precast concrete beams and cast-in-place concrete slabs has been the subject of Saemann and Washa (1964) tests.

Fig. (9) shows the beam cross section used with nominal dimensions indicated. The reduced breadth of web produced high horizontal shearing stress in the bonded joint between the web and slab at loads well below flexural failure. The beams were designed to have the joint 50.8 mm (2 in.) above the neutral axis.

Fig. (10) shows the arrangement of stirrups (ϕ 12 bars) in the beam having the maximum percentage of stirrup steel across the joint. As the nominal steel percentage decreased from 1.02 to 0.51 and from 0.51 to 0.20, the reduction in the percentage of stirrup steel across the joint in each case was accomplished by cutting off half of the stirrups crossing the joint at a level 25.4 mm (1 in.) below the joint. The number of stirrups crossing the joint for a nominal steel percentage of 0.11 was the same as for 0.20 but ϕ 10 (#3) bars were used instead of ϕ 12 (#4) bars. As the nominal steel percentage decreased from 0.11 to 0.06 half of the ϕ 10 bars were cut off 25.4 mm (1 in.) below the joint. In summary, the information on the steel bars crossing the joint is given in **Table (1).** Percentage of steel was calculated by dividing the area of all stirrups crossing the joint by the total joint area.

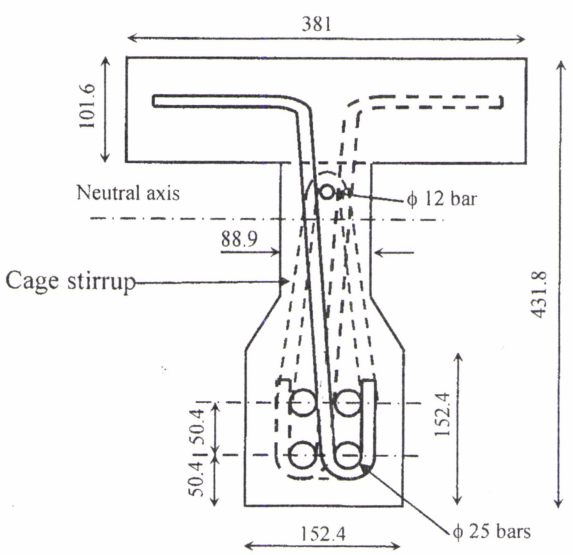

Fig. (9) Beam cross section (Saemann and Washa, 1964).

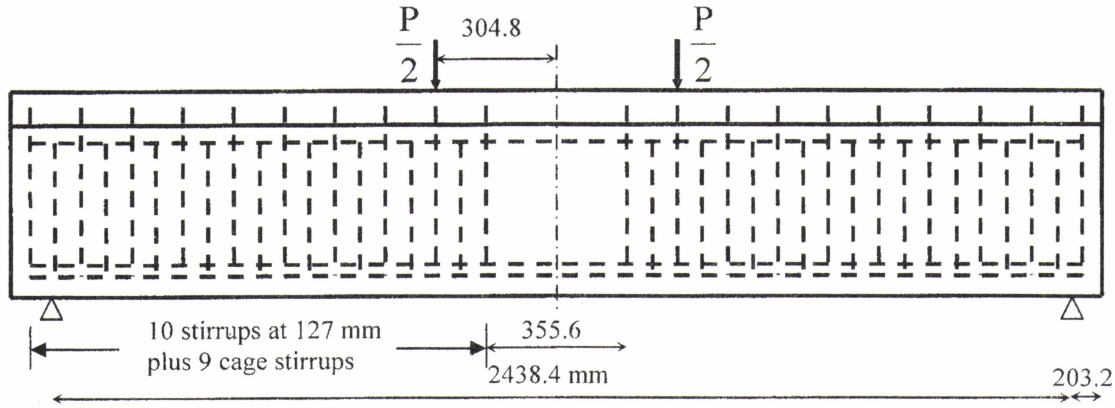

Fig. (10) Arrangement of stirrups (ϕ 12 bars) in beams having the maximum percentage of stirrup steel across the joint (Saemann and Washa, 1964)

Table (1) Stirrup data.

Beam		Nominal percentage of stirrup steel across the joint	Bar size mm	Bar spacing mm (in.)
No.	Series			
10	A	1.02	ϕ 12	127 (5)
5	C	0.51	ϕ 12	254 (10)
5	D	0.20	ϕ 12	508 (20)
12	C	0.11	ϕ 10	508 (20)
14	C	0.06	ϕ 10	1016 (40)
16	C	0.00	-	-

Properties of the reinforcing steel are given in **Table (2).** Cage stirrups were added to reduce shearing stresses below the joint. All steel members of the reinforcement were welded together.

Table (2) Properties of reinforcing steel.

Size mm	Yield point MPa	Ultimate tensile strength MPa
ϕ 10	370	560
ϕ 12	294	404
ϕ 25	252	401

Seven days after the webs were cast the slabs were cast. All beams were tested 28 days after the slabs were cast (35 days after the webs were cast). Beams were supported and loaded as shown in **Fig. (10).**

The measured central deflections with respect to the applied load are shown in **Fig. (11)** for beams of 2.438 m (8 ft) clear span, and with different percentage of steel across the joint. The curves show, in general, that for an intermediate surface roughness the maximum load increased from about 232 kN to 356 kN as the percent steel across the joint increased from zero to 1.02 percent. However, the beams behavior (central deflections) were almost identical when the load is below 200 kN. This means that the reinforcement crossing the joint (stirrups) has no observable effect on the composite beam behavior as the bond between the two concretes is not broken, and its effectiveness begins after a crack forms in the joint (dowel action).

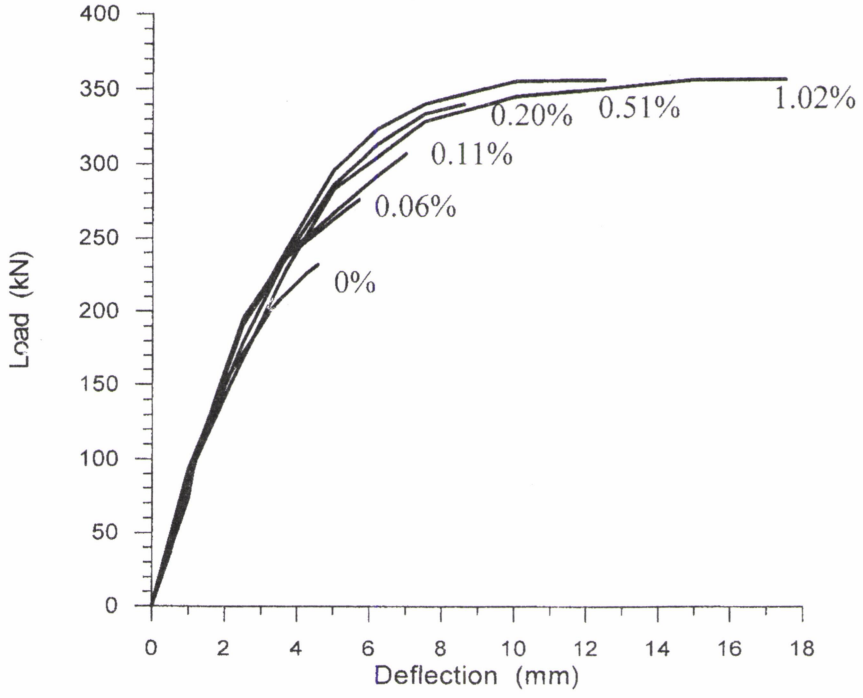

Fig. (11) Measured central deflection with respect to the applied load for beams with different percentage of steel across the joint.

Finite element idealization:

Due to symmetry, both in geometry and loading in the beams tested by Saemann and Washa (1964), only halves of the beams are idealized by restraining the horizontal movement of the nodes at the beam centerline.

Fig. (12) illustrates the finite element mesh for 2.438 m (8 ft) beam having the maximum percentage of stirrup steel across the joint. Concrete is idealized by using 198 four-noded plane stress elements. Reinforcement is idealized by 178 truss bar elements. 143 bond-slip linkage elements of zero length are used to represent the bond-slip between concrete and steel. The joint between the web and slab is idealized by 23 shear-friction interface elements and 10 dowel linkage elements. The total number of nodes resulting from the above idealization is 396 nodes.

An incremental load is applied at node 310. The number of increments depends on the ultimate strength of the beam, and ranges between 40 and 50 increments.

Discussion of results:

Fig. (13) shows the experimental and the finite element results of six beams having different percentages of steel across the joint. The same trend of behavior is seen for the numerical and the

test results, but the finite element results show less value. This may be attributed to the selfweight effects on the stresses and strains, which were neglected in the analysis.

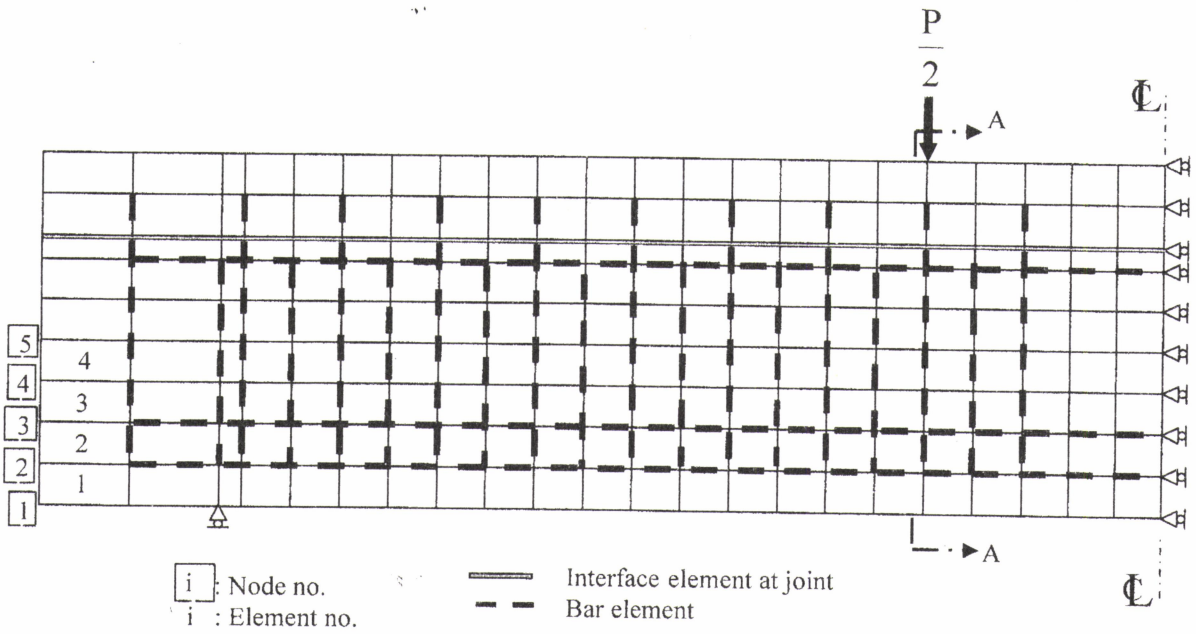

Fig. (12) Finite element discretization of a beam tested by Saemann and Washa.

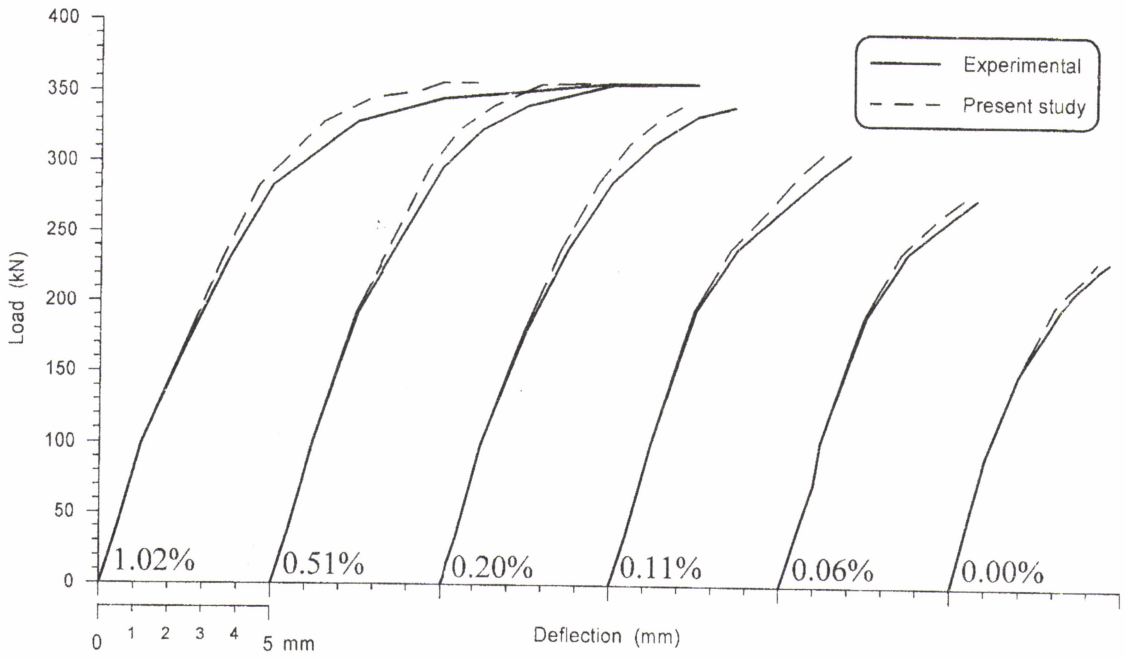

Fig. (13) Comparison between experimental and present study results.

As the shear caused slip to develop between the flange and the web, the beam began to act as a partially composite member. This action is shown in **Figs. (14) and (15)** where the computed normal strain distribution at Section A-A refer to **Fig. (12)** in beams 16C and 10 A, respectively, is plotted for a series of increasing loads. It may be noted that from the beginning a discontinuity in the strain distribution at the joint is apparent. This discontinuity is pronounced as the load increases and it is apparent that two-beam action exists. The neutral axis of the composite beam remains in its position although the load increases. This behavior results from the tendency of the beam and the slab to act separately.

Figs. (16) and (17) show the horizontal normal stresses (in X-direction) at section A-A They show gradual deviation from the linear behavior, especially where the stresses are high, indicating the nonlinear nature of concrete behavior. The crack propagation is clear with the increase of the applied load. The stress distribution shows that the composite concrete beam acts as a partially composite beam from the first load increment. This is due to the relative movement between the two concretes at the surface between them.

Prediction of cracking by the finite element method at the ultimate load for beam 16C (zero percentage of steel) is shown in **Fig. (18).** The overall depth and pattern of the cracks indicate that the failure is due to shear failure between the two concrete parts (at the joint). This result agrees with the type of failure observed experimentally by Saemann and Washa (1964).

The cracking and failure mechanism of the joint were similar for all beams analyzed in this section. The usual crack due to a combined state of bending and shear developed in the shear span of the precast beam. These cracks started as vertical cracks and turned more and more towards the load point as the loading progressed. In general, the cracks stopped when they reached the horizontal joint. However, after additional loading some of the cracks continued horizontally below the contact surface towards the load point. Examination of failure done by Saemann and Washa indicated that in most cases some concrete from the web adhered to the flange.

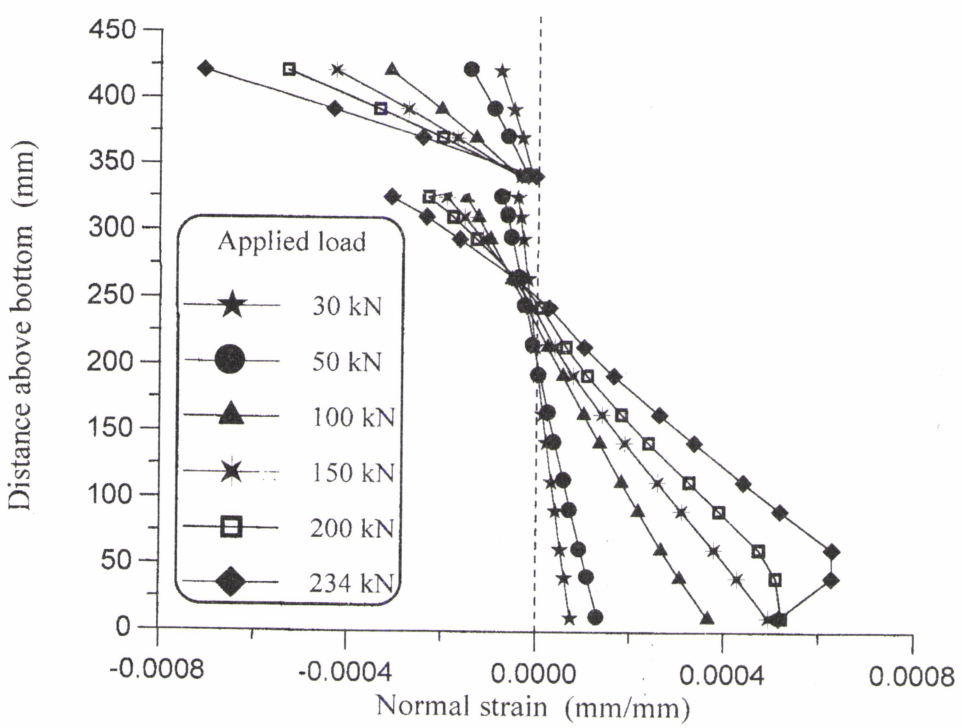

Fig. (14) Normal strain distribution at section A-A in beam with 0% steel across the joint, showing two-beam action.

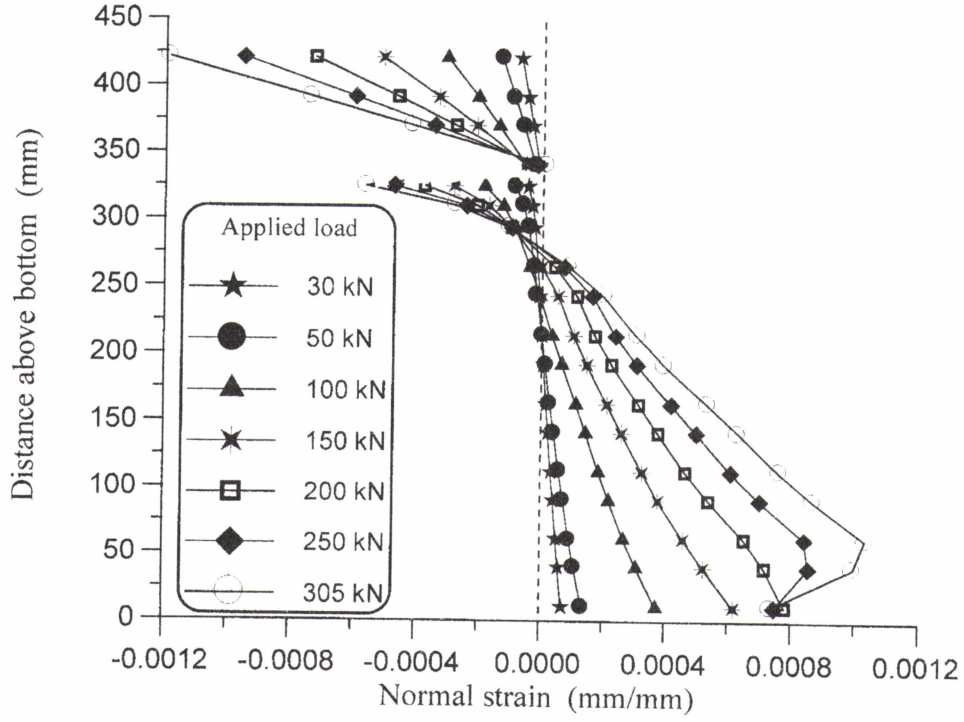

Fig. (15) Normal strains distribution at section A-A in beam with 1.02% steel across the joint, showing two-beam action.

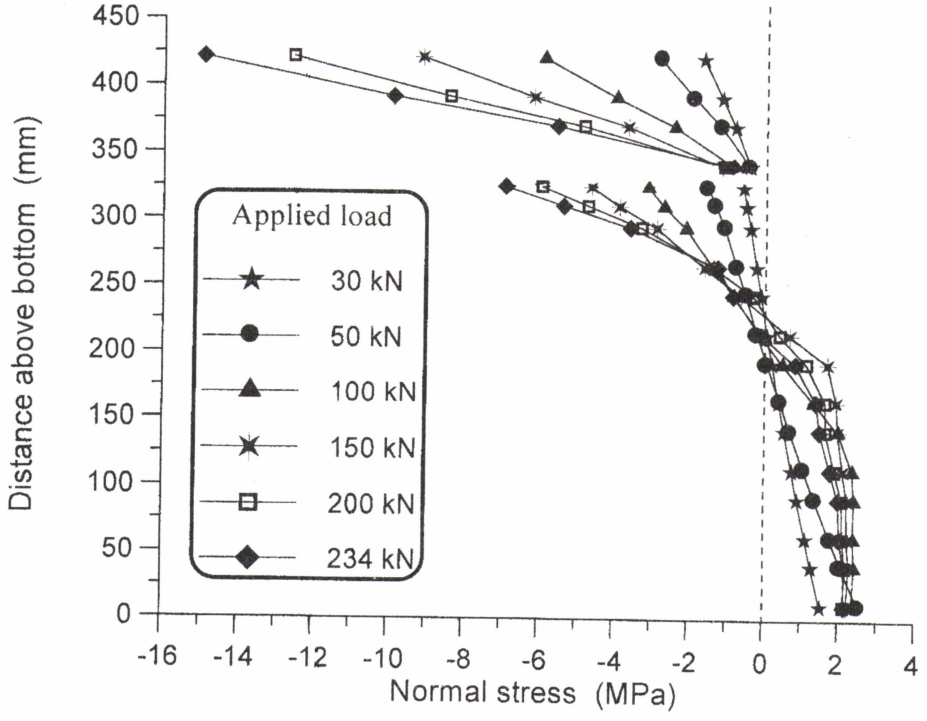

Fig. (16) Normal stresses distribution at section A-A in beam with 0% steel across the joint, showing two-beam action.

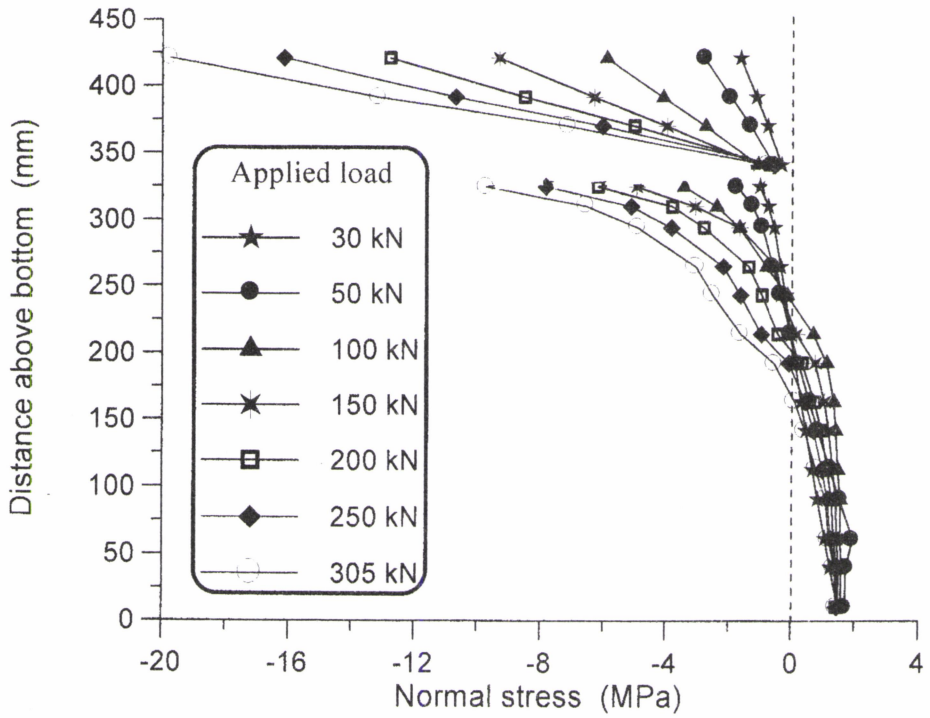

Fig. (17) Normal stresses distribution at section A-A in beam with 1.02% steel across the joint, showing two-beam action.

$\frac{P}{2}$

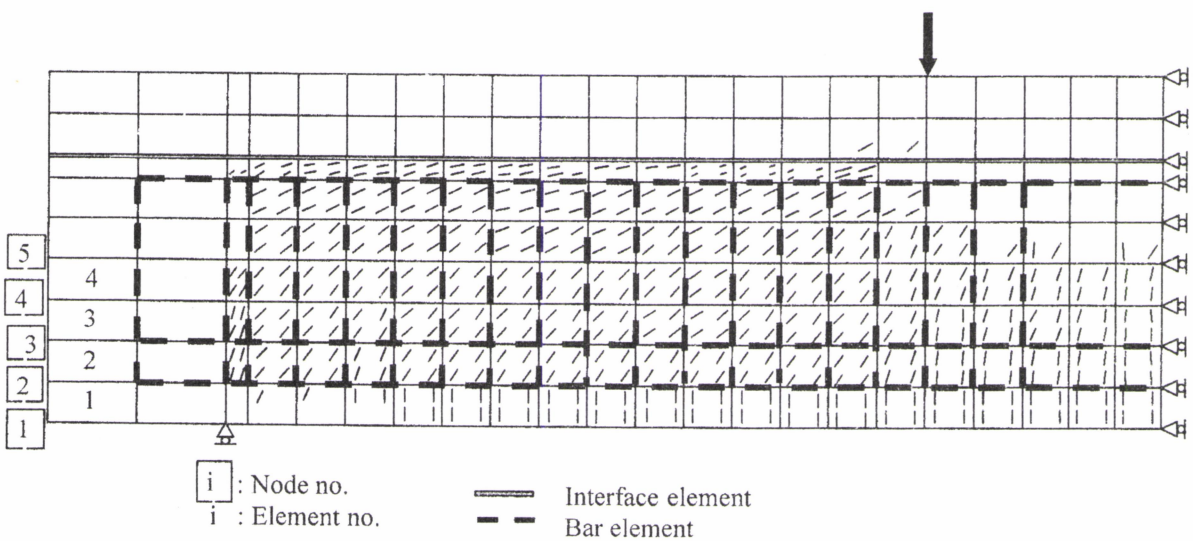

Fig. (18) Prediction of cracking by the finite element method at the ultimate load for beam 16C (zero percentage of steel).

Shearing stresses, slips, normal stresses, and separations at the joint for beam 16C (zero steel percent across the joint) and beam 10A (1.02% steel percentage across the joint) are shown in **Figs. (19) and (20),** respectively, for a series of increasing loads. The curves show that the values increased as the load increased, that maximum shearing stresses and slips were usually located about 900 mm from the left end of the beam, and that separations (loss of bond) started at relatively low load levels at the beam end. This agrees well with the results of Cook's investigation (1977) of bonded-aggregate composite beams.

Also, it can be noticed that the shearing stresses and the normal stresses between the two concretes decreased with the increase in the steel percentage across the joint.

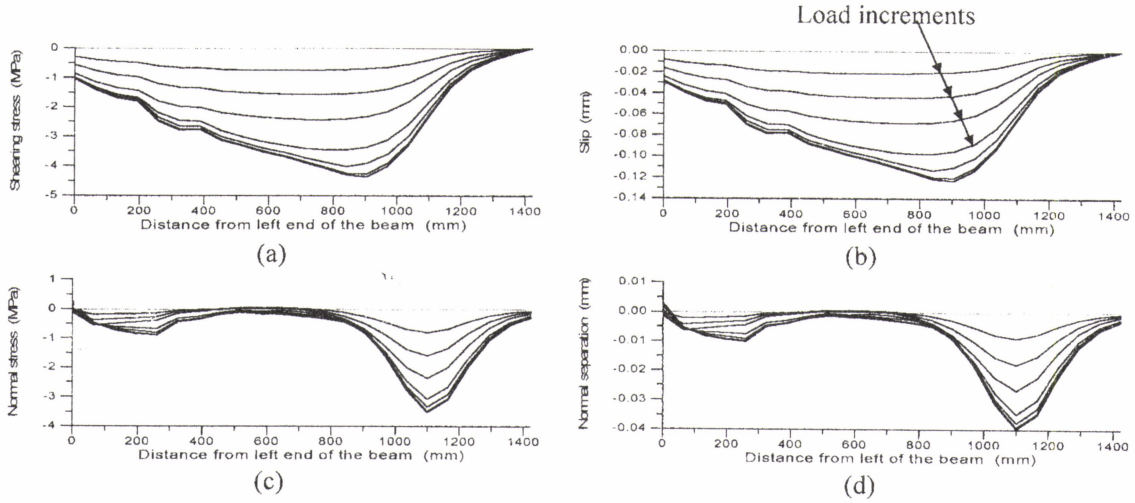

Fig. (19) Distribution of (a) shearing stresses, (b) slips, (c) normal stresses, and (d) normal separations across the joint for beam 16C (zero steel percentage) under concentrated load.

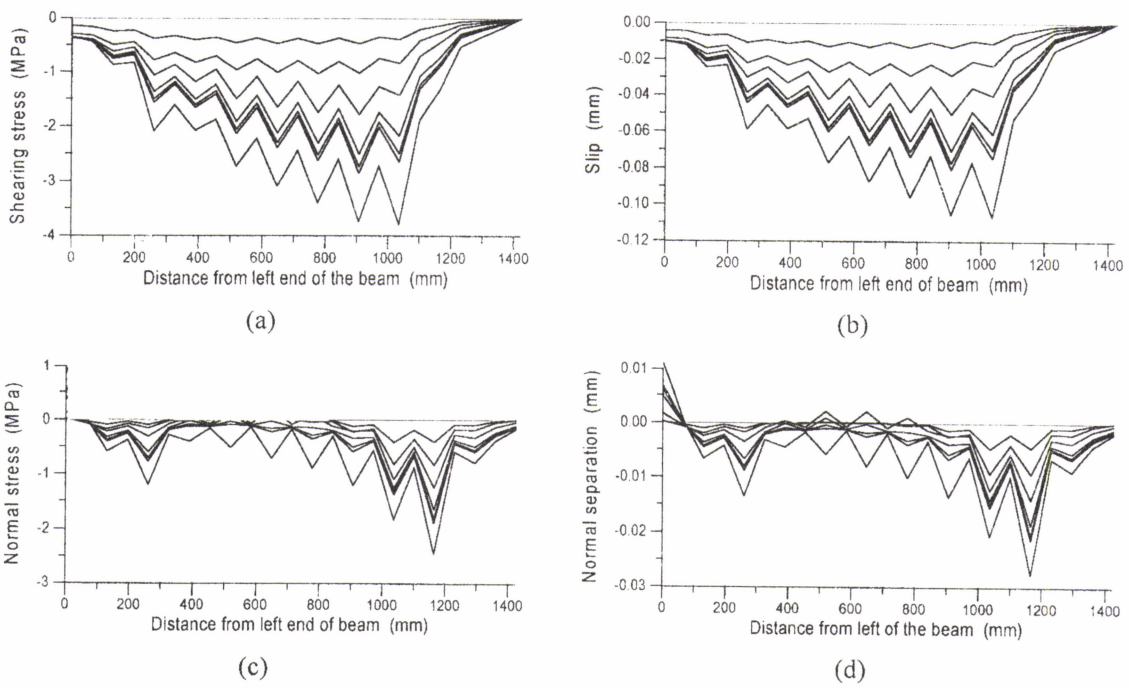

Fig. (20) Distribution of (a) shearing stresses, (b) slips, (c) normal stresses, and (d) normal separations across the joint for beam 10A (1.02% steel percentage) under concentrated load.

CONCLUSIONS

The following conclusions can be drawn from the present work:

1- A good estimate can be obtained from the analysis and ultimate load calculation of composite concrete beams that might be achieved by the Program MHND which may contribute in more practical designs.
2- The present algorithm for the analysis of composite concrete beams proves to predict beams behavior satisfactorily and indicates good estimates of failure loads compared with experimental values.
3- The performance of the linkage element and interface element, used in this study to model dowel action and shear transfer between two concretes cast in different times, is quit good.
4- Shear connectors have no observable effect on the composite concrete beam behavior at the early load stages, and their effectiveness begins after a considerable slip occurs between the precast beam and the cast-in-place slab.
5- From the early load stages, as the shear causes slip to develop between the web and the flange, the composite beam behaves as a partially composite member.

REFERENCES

ACI Committee 318, (1995). "Building Code Requirements for Structural Concrete (ACI 318-95)." American Concrete Institute, Detroit,.

Al-Sherrawi, Mohannad H. (2000). "Shear and Moment Behavior of Composite Concrete Beams." Ph.D. Thesis, Dept. of Civil Eng., Univ. of Baghdad, 135.

Darwin, D., and Graham, E. K. (1993). "Effect of Deformation Height and Spacing on Bond Strength of Reinforcing Bars." ACI Struct. J., 90(6), 646-657.

Dei Poli, S., Di Prisco, M., and Gambarova, P. G. (1993). "Cover and Stirrup Effects on the Shear Response of Dowel Bar Embedded in Concrete." ACI Struct. J., 90(4), 441-450.

Fronteddu, L., Léger, P., and Tinawi, R. (1998). "Static and Dynamic Behavior of Concrete Lift Joint Interfaces." J. Struct. Engrg., ASCE, 124(12), 1418-1430.

Mills, G. M. (1975). "A Partial Kinking Criterion for Reinforced Concrete Slabs." Mag. Concrete Res., 27(90), 13-22.

Pauley, T., Park, R., and Phillips, M. H. (1974). "Horizontal Construction Joints in Cast-in-Place Reinforced Concrete." Shear in Reinforced Concrete, Detroit, American Concrete Institute, ACI Special Publication SP-42. 2, 599-616.

Saemann, J. C., and Washa, G. W. (1964). "Horizontal Shear Connections between Precast Beams and Cast-in-Place Slabs." ACI J., 61(11), 1383-1409.

Vecchio, F. J., and Collins, M. P. (1986). "The Modified Compression Field Theory for Reinforced Concrete Elements Subjected to Shear." ACI J., 83(2), 219-231.

NOTATIONS

d_b the diameter of the bar.
E_c the modulus of elasticity of concrete.
f_{cr} the concrete cracking stress
k_d the secant stiffness of dowel action against core.

k_s the secant stiffness of bond-slip.
Δ the dowel displacement.
Δ_s the slip between steel and concrete.
χ_i the interface roughness factor.
ε_c the average principal compressive strain in concrete.
ε_{cr} the concrete cracking strain.
ε_o the strain in concrete cylinder at peak stress of concrete.
ε_{cr} the average principal tensile strain in concrete.
λ_d the dynamic reduction factor.
μ the coefficient of friction.
μ_b the basic friction coefficient.
k_s the roughness friction coefficient.
σ_c the average principal compressive stress in concrete.
σ_n the normal stresses.
θ the average principal tensile stress in concrete.
μ_b the strain softening coefficient of concrete.
ζ_σ the stress softening coefficient of concrete.